The Protonation State of the Glu-71/Asp-80 Residues in the KcsA Potassium Channel: A First-Principles QM/MM Molecular Dynamics Study

Denis Bucher,*[†] Leonardo Guidoni,*[‡] and Ursula Rothlisberger*

*Federal Institute of Technology EPFL, Institute of Chemical Sciences and Engineering, Lausanne, Switzerland; [†]The University of Sydney, School of Physics A28 and Chemistry F11, Sydney, Australia; and [‡]Universita' degli Studi di Roma "La Sapienza", Physics Department, Rome, Italy

ABSTRACT   Although a few x-ray structures of the KcsA K$^+$ channel have been crystallized several issues concerning the mechanisms of the ionic permeation and the protonation state of the selectivity filter ionizable side chains are still open. Using a first-principles quantum mechanical/molecular mechanical simulation approach, we have investigated the protonation state of Glu-71 and Asp-80, two important residues located in the vicinity of the selectivity filter. Results from the dynamics show that a proton is shared between the two residues, with a slight preference for Glu-71. The proton is found to exchange on the picosecond timescale, an interesting phenomenon that cannot be observed in classical molecular dynamics. Simulations of different ionic loading states of the filter show that the probability for the proton transfer is correlated with the filter occupancy. In addition, the Glu-71/Asp-80 pair is able to modulate the potential energy profile experienced by a K$^+$ ion as it translates along the pore axis. These theoretical predictions, along with recent experimental results, suggest that changes of the filter structure could be associated with a shift in the Glu-Asp protonation state, which in turn would influence the ion translocation.

INTRODUCTION

Ionic channels are membrane proteins that regulate a vast range of physiological processes. In particular, they are important in shaping the action potential, and in determining the neuronal excitability and plasticity (1). A variety of mechanisms regulate the channel gating (i.e., the opening and closing probability), such as transmembrane voltage, ligand binding, mechanical stress, and pH. K$^+$ selective channels are widely spread in all organisms and have the ability to conduct K$^+$ ions at near diffusion limit ($\sim 10^8$ ions s^{-1} channel^{-1}) while remaining very selective toward other monovalent cations like Na$^+$ (2). In recent years, three-dimensional structures of ion channels from different organisms solved by x-ray crystallography have shed light on the molecular mechanisms of permeation, selectivity, and gating (3–5). Among these channels, the KcsA K$^+$ channel from *Streptomyces lividians* turned out to be a specially good candidate for high-resolution x-ray structural measurements under different conditions of permeant cation and ionic concentrations (6).

The KcsA channel shares sequence and structure similarities with all members of the K$^+$ channel family. Main features of all K$^+$ channels, like the conformation of the conserved TVGYG sequence motif that forms the selectivity filter, are therefore well represented by this small bacterial channel. The KcsA K$^+$ channel is a tetramer. Each subunit contains two transmembrane helices (M1 and M2) with an intervening loop made up of a short helix (P loop). A water-filled cavity is present at the middle of the membrane. This intracellular vestibule is located at the entrance of the selectivity filter and stabilizes the permeant ions (Fig. 1). Two distinct and equivalently populated K$^+$ loading states of the selectivity filter were detected by x-ray crystallography (7). Following the notation introduced by Aqvist (8) they are the (1010) state (hereafter referred to as A) and the (0101) state (hereafter referred to as B).

In the KcsA channel, two ionizable residues are located in the vicinity of the filter (Fig. 1, *right panel*), Glu-71 and Asp-80. To build an accurate model of ion permeation in KcsA, it is important to determine the protonation state of these residues. Recent 2.0-Å resolution data (1K4C) (5) revealed that the Glu-71 side chain (not determined in the previously reported x-ray structure (3)) is involved in a carboxyl-carboxylate linkage with Asp-80, and that the two residues stabilize a water molecule. The buried Glu-71 residue is coordinated to the filter through an H-bond pattern involving amino acids Gly-77, Tyr-78, and Val-76, whereas the Asp-80 residue is located in the outer mouth of the channel on the distal side of the signature sequence. The Asp-80 side chain is accessible to the external solution.

The protonation state of the two residues is an important issue for the theoretical study of ion permeation within the KcsA channel, because it affects the potential energy profile along the selectivity filter (9). Another key issue concerns the interplay between Glu-71/Asp-80 and the nearby Arg-89 of the neighboring monomer (10–14). Although Asp-80 side-chain neutralization severely compromises the KcsA oligomeric stability, Glu-71-Val mutation, does not influence ionic selectivity but alters channel stability and single channel conductance (15). In addition, recent experimental studies suggest that Glu-71 and Asp-80 residues play a role in the voltage-gating process of the KcsA channel (11,12,16,17) and
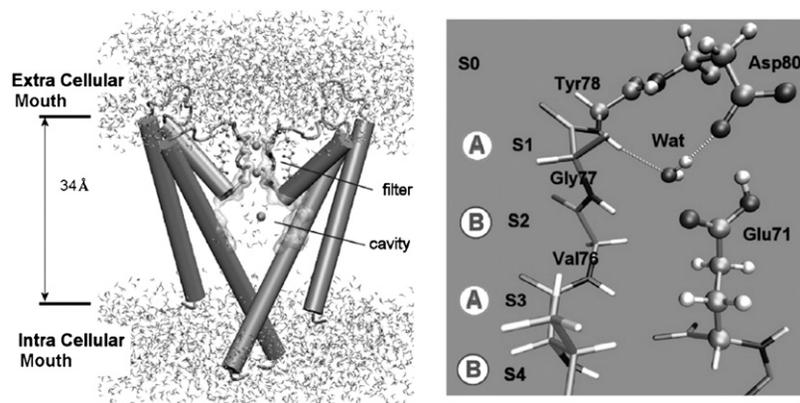

FIGURE 1 Snapshot from the simulation. (*Left panel*) Schematic diagram of the simulated system. Two channel subunits are shown as cartoon, K^+ ions as spheres, bulk and cavity water molecules as sticks. The region indicated by the arrow is immersed in *n*-octane (not shown). (*Right panel*) Details of the selectivity filter. The residues Glu-71/Asp-80 are in the vicinity of the selectivity filter fingerprint. The location of the K^+ binding site (S_1–S_4) inside the selectivity filter is indicated. Two distinct loading states of the filter were investigated in the simulations: (*A*) ions in S_1, S_3, water in S_2, S_4; and (*B*) ions in S_1, S_4, water in S_1, S_3.

in the coupling between gating and permeation in the KcsA and KirBac channels (18–20).

The exact protonation state of the acid dyad has been the subject of several contradicting theoretical studies (8,9,21, 22), but it remains experimentally unknown. In classical simulations of the KcsA channel, the Glu-71/Asp-80 di-acid pair has been simplified by considering one of the two residues in its protonated form and the other in its deprotonated form. The most common assumption in computational setups has been to consider Glu-71 as protonated, allowing for the deprotonated Asp-80 to interact with both solvent and Arg-89 (23–27). In some earlier simulations, the default ionization state at neutral pH was used (i.e., both residues were deprotonated) (28–30).

Previous attempts to attribute the protonation state of the Glu-71/Asp-80 residues have been based on classical force fields. However, an important limitation of these studies is that the parameters used for the description of the Glu-Asp di-acid pair were not developed for residues involved in a strong hydrogen bond where polarization effects play a role (31). This view is supported by ab initio calculations at the HF 6-31G** level showing that the partial charges of the proton and of the neighboring carboxylate oxygens may vary by ~0.05–0.10 unit charges if the two fragments are considered separately or together, respectively (21).

Nonpolarizable force fields also neglect the influence of the moving ions on the partial charges neighboring the Glu-71/Asp-80 residues. Yet, small differences in the force field parameterization are sufficient to affect significantly the outcome of pKa calculations based on Poisson-Boltzmann calculations (PB) or molecular dynamics (MD) free energy sampling (MD/FES) (32). Using PB pKa calculations, Ranatunga et al. found that Glu-71 is more likely to be protonated at pH 7 when no ions are present in the filter. However, protonation of Asp-80 is favored ~1.5–2 kcal/mol if two K^+ ions are present in the selectivity filter. Since it is very likely that at physiological conditions the selectivity filter is occupied by two ions (33), this study indicated that it is mainly Asp-80 that is protonated. Bernèche and Roux reached a similar conclusion by calculating the ionization free energy of

Glu-71 and Asp-80 for 80 configurations extracted from an MD trajectory (21). The results indicated that Asp-80 protonation is ~2 kcal/mol more stable on average, with large root mean square deviations (RMSD) of 2–3 kcal/mol. Therefore these two studies indicated a possible protonation of Asp-80. However, to the best of our knowledge, this choice was never used in any of the atomistic MD simulations of KcsA. Luzhkov and Aqvist (8,22), on the other hand, found that protonation of Glu-71 was more stable on the basis of MD/FEP calculations. Their results indicated that protonation of Asp-80 is less favorable by ~2–3 kcal/mol. In summary, classical studies have suggested that one of the two residues is protonated; however, they are not conclusive in assigning the protonation state.

To address the question about the ionization state of the Glu-71/Asp-80 residues, we have used a quantum mechanical/molecular mechanical (QM/MM) simulation scheme where the two residues and their surroundings are treated by first principle molecular dynamics whereas all the rest of the protein and environment is described at the force-field level. Anticipating our results, we observe that proton transfer occurs between the two di-acid residues on the picosecond timescale. The effect of the environment on the proton hopping has been investigated. In addition, we show that the protonation state influences significantly the K^+ ion stabilization energy in the filter.

METHODS

Structural models

Our simulation systems are based on the x-ray structure of Zhou et al. (5) (Protein Data Bank (PDB) entry 1K4C). The crystal structure was immersed in a preequilibrated water-octane (73.6 × 73 ×73 Å) box. This approach supplies a stable hydrophilic-hydrophobic liquid interface quickly adaptable to the protein and has been successfully applied previously to transmembrane channel models (34) and to KcsA (13,35). Following the latter works, the water-hydrocarbon interface is located between Trp-87 and Thr-85 (extracellular side) and between Trp-113 and Arg-117 (intracellular side). This choice, suggested by Doyle et al. (3), is in good agreement with electron paramagnetic resonance data (36). Four Na^+ ions and 18 Cl^- ions were added, which corresponds to a ionic strength of ~50 mM.

Simulation systems

Starting from the structural model described above we built up different simulation systems including classical and QM/MM systems. We have treated the Asp/Glu pair and the most relevant nearest residues at the quantum level whereas all the rest of the protein, membrane environment, and water solution have been treated at force-field level. In particular, the quantum system was composed by the Glu-71 and the Asp-80 side chains, and the crystallographic water molecules. According to the K^+ ions loading state and to the proton location on the Asp-Glu dyad, different simulation systems were set up: A), Selectivity filter loading state (1010), namely with ions put in S_1, S_3 and water molecules in S_2 and S_4 (see Fig. 1); B), selectivity filter loading state (0101), namely ions are put in S_2, S_4 and water molecules in S_1, S_3; and C), Gas phase system. This system includes in addition to the Asp-Gly dyad, the backbone of amino acids Gly-77, Tyr-78, Gly-79, Leu-81, the crystallographic water, and a potassium ion in the S_1 or S_2 crystallographic position. Hydrogen capping was used to close the open valences.

Classical MD simulations

Energy minimization of the fully solvated protein was carried out followed by a 0.1-ns equilibration period where the protein backbone and the cation positions were restrained. After this, MD simulations were performed in the NVT ensemble for 0.5 ns. Berendsen thermostat was used at 100 K, with a time constant for heat bath coupling of 1 ps. The simulations were performed at 100 K, the experimental temperature for the determination of the crystal structure 1K4C, in an attempt to assign the protonation state of the high resolution x-ray structure of KcsA (5). In addition, simulations at physiological temperature (310 K) were carried out. The following cutoffs were used for long-range interaction: 10 Å for van der Waals interactions and 12 Å for the real space part of the electrostatic interactions. Periodic boundary conditions were applied and electrostatic interactions were calculated with the particle mesh Ewald summation method (37). All the classical MD simulations were carried out using the AMBER 7.0 suite of programs (38).

QM/MM simulations

All systems were equilibrated by extensive classical MD simulations. The density functional theory (DFT)-based Car-Parrinello (39) molecular dynamics program CPMD (40) v.3.8 was used for the QM/MM (41) simulations of KcsA. The quantum problem was solved using DFT, in the formulation by Kohn-Sham (42), using the local density approximation with BLYP gradient corrections (43,44). The core-valence electron interactions were described using Martins and Trouiller pseudopotentials (45). The Kohn-Sham orbitals were expanded in a plane wave basis setup to a cutoff of 70 Ry. The electronic wave functions were optimized up to a maximal change in the Kohn-Sham energy lower than 0.0006 kcal/mol. The time step for the dynamics was 0.097 fs and the fictitious electron mass was chosen to be 600 a.u. The size of the orthorhombic QM box was $11.7 \times 10.6 \times 16.4$ Å. A Nosé-Hoover thermostat was used with a coupling frequency of 1200 cm^{-1} to maintain a constant temperature. In total, six QM/MM simulations were performed. Two simulations were carried out for 2 ps on: I), A_GLUH and II), A_ASPH, at 100 K. Two longer simulations were carried out on A and B, at 100 K, each lasting 12 ps. In addition, two 6-ps simulations were performed on A and B at physiological temperature (310 K).

Gas phase optimizations

Single point energy calculations and geometry optimizations on cluster models of the Glu-71 and Asp-80 residues were performed, using the Gaussian03 package (46), at the BLYP level of theory with the 6–31G* basis set.

Electrostatic potential analysis

The electrostatic potential was calculated by first principles QM/MM methods on the x-ray structure of Zhou et al. (5) (PDB entry 1K4C). The QM box contained a total of 160 atoms, which included the conserved amino acids of the TVGYG sequence of the four identical subunits of the KcsA channel. The size of the orthorhombic QM box was $15 \times 15 \times 30$ Å. The two K^+ ions and the two water molecules inside the selectivity filter were removed. The electrostatic potential was computed twice: once with all four Glu-71 and once with all four Asp-80 protonated.

RESULTS

In the following sections, the potential energy surface of the proton transfer reaction between Glu-71 and Asp-80 is explored and the stabilizing role of the environment is discussed. Next, the impact of the proton transfer on the ion stabilization energy inside the filter is investigated.

Ionization state in the x-ray structure

Which residue is protonated in the Glu-71/Asp-80 di-acid pair? To answer this question, two QM/MM simulations starting from model A and B at the crystal temperature of 100 K were carried out. Three to five proton exchanges were observed during the course of the simulations (12 ps). In Table 1, the agreement between the simulated structure and the x-ray data is reported for representative distances of the network of H-bonds that connect the filter to Glu-71 and to Asp-80. We find that when a constraint is applied to the O-H bond to fix the protonation state, the average deviation from the x-ray structure is larger. Indeed, the agreement between experimental and simulated structures is maximized by allowing the proton to swap. The agreement with

TABLE 1 Selected distances representative of Glu-71/Asp-80 interaction with the selectivity filter in the x-ray data and QM/MM simulations

Structure	Glu-71:O Gly-79:N	Glu-71:O Tyr-78:N	Asp-80:O Tyr-78:N	Asp-80:O Gly-79:N	Glu-71:O' Asp-80:O	RMSD
1K4C	4.22	2.96	4.76	3.91	2.63	–
A_ASPH	4.78	3.20	4.64	4.70	2.54	1.00
A_GLUH	4.59	3.30	4.70	4.14	2.57	0.56
A + B	4.37	3.28	4.75	4.24	2.56	0.48

Simulations in the (1010) ion occupation were preformed using A_GLUH and A_ASPH, with constraints to fix the proton position. RMSD is given relative to the (1K4C/ Doyle 2001) x-ray structure. A and B represent the (1010) and (0101) loading state of the filter, respectively.

the experimental data was further increased by extending the sampling to both ion occupation of the filter (A and B), for 12 ps each, and then attributing an equal weights to the two. In this case, an average RMSD of 0.48 Å was obtained for the selected distances.

The most common assumption found in the literature is to consider the Glu-71 as protonated while the four Asp-80s are chosen as deprotonated. This assumption was tested here in classical and in QM/MM simulations. Indeed, simulations in which a constraint on the O-H bond was applied to maintain Glu-71 protonated showed better results than the fixed protonation of Asp-80. Protonation of Asp-80 produced a mean deviation of 1 Å for the selected distances of the H-bond network in the QM/MM simulations. A similar result was found in the classical simulations where A_GLUH better reproduced the structural data. In particular, the salt bridge linking Asp-80 with Arg-89 was not maintained in A_ASPH. To summarize, we find that the protonation of Glu-71 is able to better reproduce the crystallographic data (PDB entry 1K4C) (5) in MD simulations (Table 1). However, the best agreement occurs when the proton is allowed to exchange between Glu-71 and Asp-80. This phenomenon cannot be observed in force-field-based simulations. To extend our study of the Glu/Asp di-acid pair to physiological temper-

atures, two 6-ps QM/MM simulations were performed at 310 K. The difference in free energy between the two protonation states was similar to the same quantity obtained at 100 K, and the proton transfer events were observed. The average O:Asp-O:Glu distance was slightly increased from 2.58 Å, at 100 K, to 2.64 Å.

Influence of the environment

Close inspection of the QM/MM trajectories indicates possible environmental factors that could influence proton transfer probability. In the deprotonated state, Asp-80 is able to from a salt bridge with Arg-89. This salt bridge is present in crystal structures of KcsA and is believed to be critical to stabilize the channel architecture (13,15). Additional stabilizations of the charged Asp-80 come from the N-H backbone dipoles of Asp-80 and Gly-81. On the other hand, different factors favor a transfer of the proton to Asp-80. They are: i), the orientation of the buried water molecule, which is able to rotate its dipole moment by ~90° to accommodate the proton transfer; and ii), the favorable interactions between ions in the selectivity filter and the deprotonated Glu-71 side chains. The latter two effects will be discussed in the next subsections.
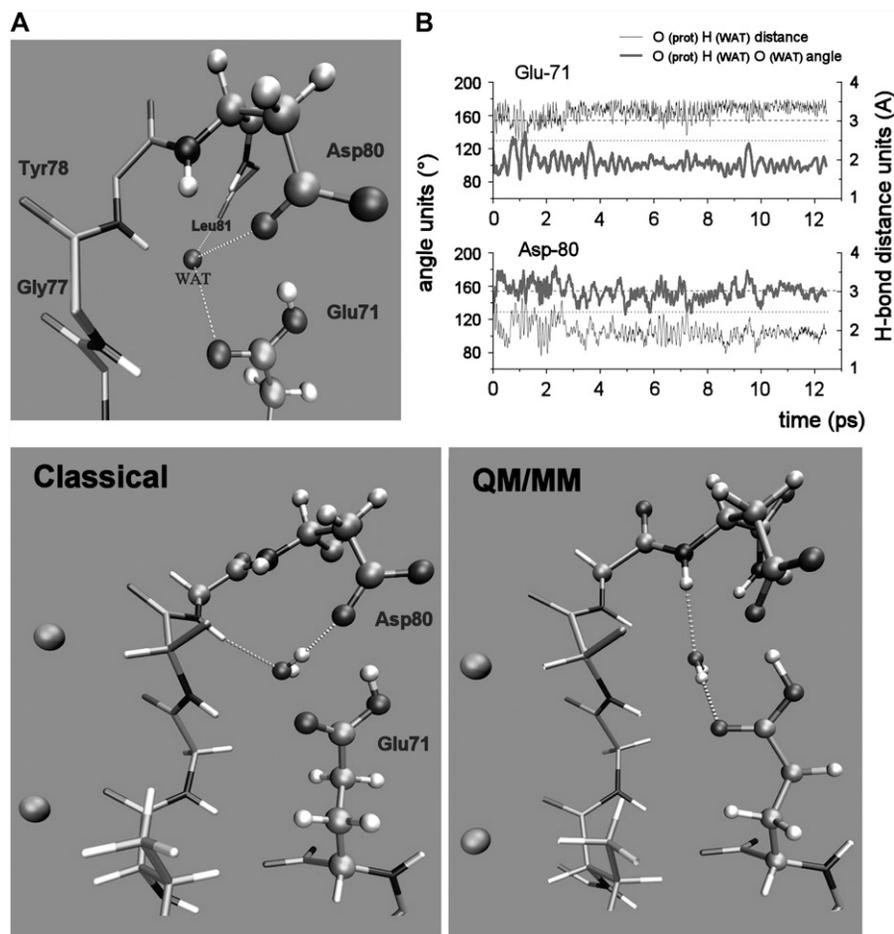

FIGURE 2 (Top) Orientation of the crystallographic water molecule (WAT). (A) H-bond acceptors (dotted lines) with O–O distances to Leu-81 (2.67 Å); Glu-71 (2.91 Å); Asp-80 (3.21 Å) in the x-ray structure. (B) Interaction of WAT with the residues Glu-71/Asp-80. An H-bond was considered formed if the distance O–H(wat) (solid dark line) was smaller than 3 Å and the angle O–H(wat)–O(wat) (solid light line) was above 130°. (Bottom) Comparison between the WAT coordination in classical and QM/MM simulations. WAT is coordinated to Glu-71 (in QM/MM) as opposed to Asp-80 (in the classical simulation). The dipole moment of the water points toward the intracore side of the selectivity filter allowing the Tyr-78 carbonyls to become more flexible and solvent exposed. A different pattern is seen in the QM/MM simulation where the water molecule is bonded to Glu-71 and Asp-80 N-H, orienting its dipole toward the extracellular side and stabilizing the Tyr-78 ring.

The role of the crystallographic water molecule

The crystallographic water (WAT) molecule in the vicinity of the Glu-71/Asp-80 residues was not resolved in the first x-ray structure of KcsA (1bl8) at 3.2-Å resolution (3). In the more recent 2.0-Å resolution structure, only the position of the water oxygen is known since protons are not detectable at this resolution. Inspection of the H-bond network around WAT suggests that it interacts with the two H-bond donors, Gly-79 and Asp-80. However, at least three different orientations of the crystallographic water molecule are possible, since residues Leu-81, Glu-71, and Asp-80 are all potential H-bond acceptors (Fig. 2 A). In the QM/MM simulations, WAT is found to be preferably coordinated to the Glu-71 side chain and to the carbonyl group of Leu-81 (Fig. 2 D). The coordination with Glu-71 was maintained throughout the 12 ps of the simulations A and B (Fig. 2 B). On the other hand, a different bonding pattern was observed in the classical simulations (Fig. 2 B), where WAT remained coordinated to Leu-81 but formed an H-bond with Asp-80 instead of Glu-71. In QM/MM trajectories, the WAT coordination was unstable when bound to Asp-80 in the initial frame. The discrepancy between the classical and the QM/MM bond pattern originates presumably from the fact that the force-field parameters display a higher charge on the Asp-80 oxygen as compared to the Glu-71. Thus, for this system, it appears that the force field overestimates the charge on Asp-80. Indeed, the charges on the aspartic acid were not optimized for a di-acid bridge (31). This charge discrepancy has a consequence for the water orientation, which is bound to the selectivity filter at the position of the Tyr-78 carbonyls. Inaccuracies in the force field in describing the Glu-71/Asp-80 residues and the buried water binding have direct consequences on the classical simulations. In classical simulations of the filter in the A state, we observed deviations from the x-ray structure in the position of the K^+ ion in the S_1 binding site that can be at least partly attributed to the inaccurate description of the buried Asp/Glu di-acid pair by the force field.

The importance of the WAT orientation and mobility in relation to the proton exchange process is revealed by the QM/MM simulations. During simulation B, proton transfers were observed after 2, 6, and 10 ps. Inspection of the trajectory reveals that proton transfers coincide with the return of WAT to its initial position, suggesting that a favorable orientation of the WAT dipole is necessary to lower the energy barrier for the proton transfer. WAT is rather mobile as can be seen from the average displacement of the residues Glu-71, Asp-80, and WAT during the simulations (Fig. 3).

Influence of the filter occupancy state

Due to the close proximity of the Glu-71 residues to the S_2 binding site (6.5–7.5 Å), it is important to determine whether the presence of ions inside the selectivity filter will influence
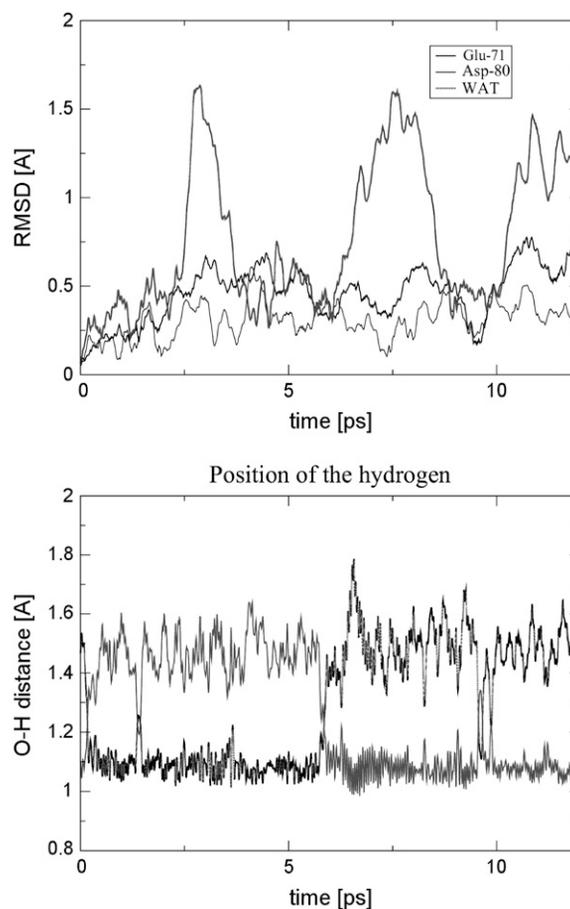

FIGURE 3 (*Top*) RMSD with respect to the first frame of the simulation for the residues Glu-71 (*dark thin line*), Asp-80 (*light thin line*), and (*WAT*) (*dark thick line*). (*Bottom*) Proton exchange between Glu-71 and Asp-80 during the 12-ps QM/MM simulation. Distance to Asp:O (*dark*) and to Glu:O (*light*).

the protonation state and vice versa. Based on PB pKa calculations, Ranatunga et al. proposed that the Glu-71/Asp-80 ionization state shows very strong dependence on the presence of K^+ ions (9). In particular, in the absence of ions in the filter, Glu-71 was predicted to be protonated. When ions were present in the selectivity filter, protonation of Asp-80 was stabilized over Glu-71 protonation by 1.5–2 kcal/mol. Because, under physiological conditions, the filter is occupied by two ions switching from the 1010 to the 0101 configuration (see Fig. 1) (7,22), it is important to decide whether the positions of these ions in the selectivity filter will influence the protonation state probability. To evaluate these effects we made a comparison between two QM/MM simulations performed on two structural models A and B only differing by the K^+ ion positions in the selectivity filter (A and B).

The results of these simulations show that the probability for each protonation state is indeed influenced by the filling state of the selectivity filter. We found that Asp-80 protonation is unlikely in state A, when the S_2 binding site is occupied by a water molecule. However, in configuration B,
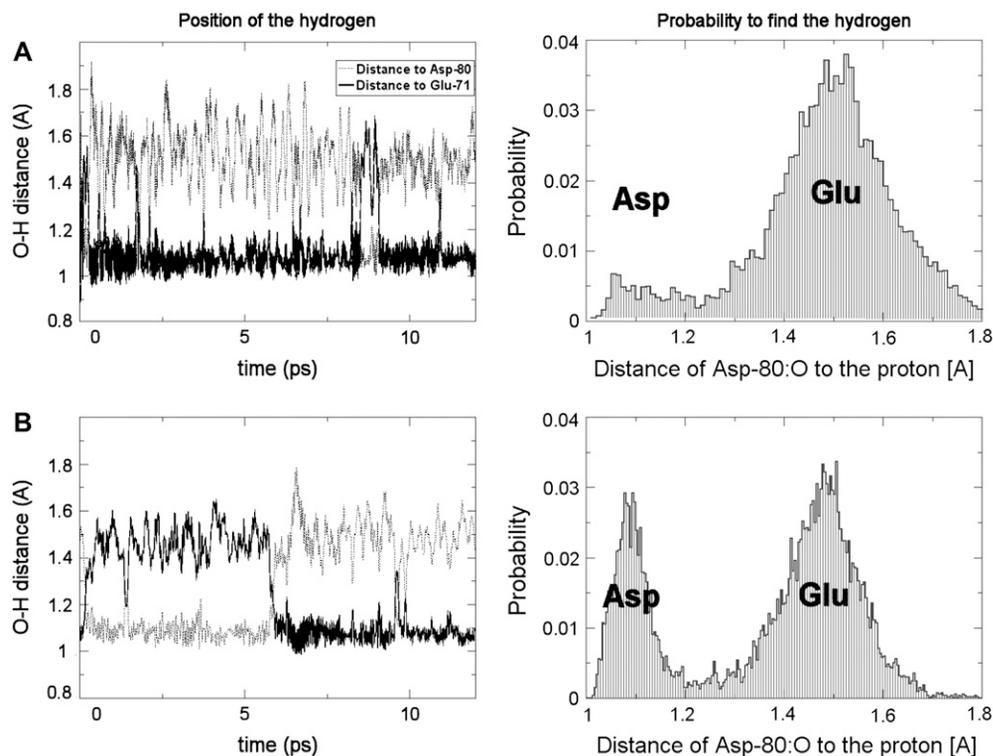
FIGURE 4 Ionization state of the Glu-71/Asp-80 pair. QM/MM simulations at 100 K starting from states A and B of the filter. (*Left panel*) Distance of the proton to the Asp-80 oxygen (*dashed*) and Glu-71 oxygen (*bold*). (*Right panel*) Histogram of the distribution of the proton at a certain distance from Asp-80 oxygen. To draw the histograms, trajectory frames were collected every 50 a.u. and put into 200 bins.

the proton was located on Asp-80 during >30% of the simulation time (Fig. 4). A probability histogram of the proton position at a given distance from Asp-80:O is shown for the two states of the filter (Fig. 4, *right panel*). The maximum of the probability function occurs at a H to Asp-80:O distance of 1.52 and 1.48 Å for state A and B, respectively, providing further indication that the instability of the Glu-71 protonation is increased in state B. The free energy profile along the O–H–O coordinate was derived from the logarithm of the proton position probability function. In the (0101) state (i.e., B), the energy of both protonation states was roughly equal. On the other hand, in the (1010) conformation A, protonation of Glu-71 was favored by 0.5–1.5 kcal/mol. This result is reproduced by cluster calculations at the DFT/BLYP and B3LYP level of theory (Fig. 5). The energy profiles along the O–H–O coordinate calculated with the BLYP and B3LYP functionals are in good agreement with the QM/MM simulations. Interestingly, a similar low activation energy is observed for the proton transfer in dibenzoic acid (47). In that case, proton tunneling effects were found to dominate the reaction rate at low temperature. Although the current methodology describes the hydrogen nucleus classically, it is expected to be accurate at physiological temperature, where thermal fluctuations dominate the reaction rate.

In summary, the QM/MM simulations of two different occupancy states of the filter (A and B) suggest that the stability of the protonated Asp-80 residues depends mainly on the occupancy of the S_2 binding site. An ion present at the outer mouth, on the other hand, would have an opposite

effect. Using a simple Coulomb Law (with $\epsilon = 2$ for the protein, and $\epsilon = 78.4$ for water), we estimate that an ion in S_0 would stabilize the Glu-71 protonation state versus the protonation of Asp-80 by ~0.5 kcal/mol.

Electrostatic energies inside the filter

KcsA is a tetramer and therefore four concerted proton transfers can occur as a response to the entrance of an ion in
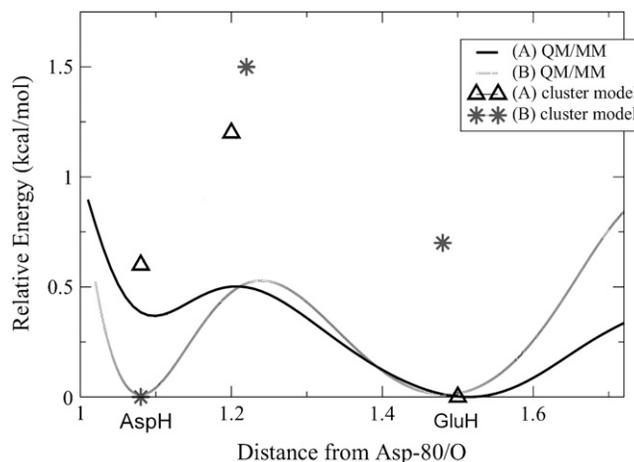

FIGURE 5 Reconstructed free energy profiles (ΔG) for the two QM/MM simulations for state A (*solid line*) and B (*dashed line*). Gas phase ΔE calculations at the BLYP level, shown on the same plot, are in qualitative agreement with the QM/MM first principles simulations.

the S_2 binding site. In Fig. 6 *A*, we show the influence of the four transfers on the electrostatic potential inside the channel. Upon proton transfer from Glu-71 to Asp-80, the potential becomes significantly more negative at the outer-mouth near the S_0 binding site (7–8 kcal/mol) (Fig. 6, *A* and *C*). In addition, after the transfer, the electronic density on the Gly-76 and Tyr-77 backbone atoms of the filter is polarized (Fig. 6 *B*) and the H-bond between Glu-71 and the N-H group of Tyr-78 becomes stronger. This polarization of the electronic density on the Gly-76 and Tyr-77 residues is similar in magnitude to the direct metal ion induced polarization (48,49).

DISCUSSION

Biological role of the di-acid bridge

The electrostatic energy shows the influence of the proton transfer on the ion stabilization along the permeation pathway. Several mechanisms may be influenced by changes in the proton transfer probability, for instance: i), the stabilization of low and high affinity conformations of the selectivity filter (50–52); ii), the voltage dependence of the channel gating (16,17); and iii), the energetical coupling between

external and internal ions, known as the ''*trans*-knock effect'' (53–56).

Since ion currents can be recorded directly in single channel experiments, the K^+ channel offers a unique opportunity to test theoretical predictions by direct measurements of the ion conduction. Several functional studies have been carried out on K^+ channels: measurements on KcsA, MthK, KvAP, and KirBac (16,57–60) have provided a vast amount of experimental data. In the context of an investigation of the Asp/Glu di-acid protonation state in KcsA, a recent functional study on the Glu-71–Val mutant (15) is particularly interesting. The tetrameric conformation was retained in the mutant, and important properties such as electrical activity and K^+/Na^+ selectivity were unaltered when reconstituted into planar lipid bilayers. Interestingly, inward conductance was increased in the mutant. The author suggested that, due to the disruption of the carboxyl-carboxylate bond in the Glu-71–Val mutant, the Asp-80 side chain may no longer be stabilized in the protein core and its influence would become pronounced at the outer surface. The absolute changes in rate constants found in this study reflect small changes in free energy of ~2 kcal/mol. In addition, the recordings of inward currents through wild-type KcsA were noisy, suggesting that the channel is undergoing a very rapid gating that is not
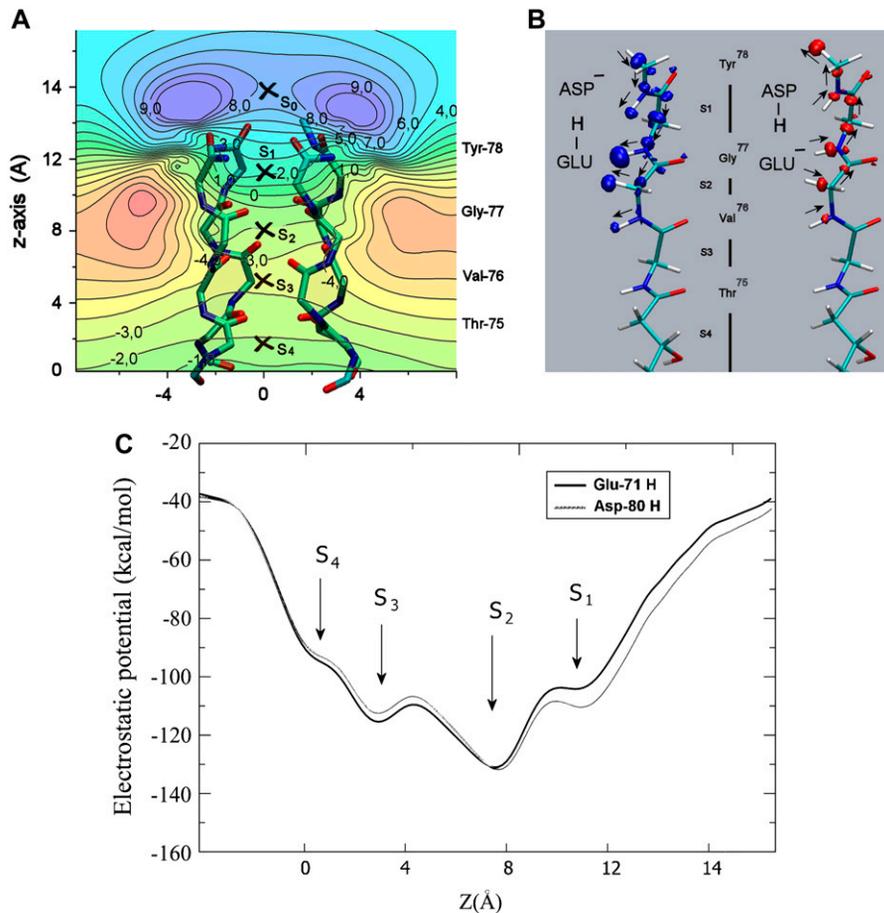

FIGURE 6   (*A*) Isopotential energy contours for a point charge inside the selectivity filter. The difference between the protonation of all four Glu-71 and all four Asp-80 residues is shown in kcal/mol. The binding sites S_0–S_4 are indicated by a cross. The origin of the *z* axis is taken at the entrance of the filter at the position of the Thr-75 OH side chains. (*B*) Isocontour with isovalue of 0.002 e/au^3 of the electronic density difference map between the two protonation states. Positive value of the electronic density difference (*left*) and negative values (*right*). Only the backbone atoms of the filter in one subunit of the channel are shown. (*C*) Electrostatic potential along the selectivity filter K^+ ions pathway. The four internal binding sites S_1–S_4 are indicated by arrows.

completely resolved by the recordings (51). Currents through the main conductance state of the Glu-71–Val channel are found to be less noisy (15). Instead, the noise recorder in the experiment may indicate that the protonation state in wild-type KcsA is modified by the different subconductance state of the filter (millisecond timescale). This mechanism could play a role in modulating inward currents in the selectivity filter. The influence of the charged Asp-80 on K^+ ions at the outer mouth of the channel is already well established experimentally (61,62). In the BKCa channel, for instance, the substitution of the aspartic acid with a neutral residue led to outward conductance reduced by only 40%. The inward conductance, on the other hand, was reduced to a much greater extent.

In summary, both experimental and theoretical predictions suggest that the Glu-71 to Asp-80 proton transfer mechanism is likely to assist the primordial function of the KcsA channel, which is the regulation of ion homeostasis (63). Although the Glu-71/Asp-80 di-acid bridge is not conserved in eukaryotic K^+ channels (64), sequence alignment studies indicate that the negatively charged amino acids that surround the selectivity filter are generally conserved within K^+ channels families. Glu-71 is conserved in inward-rectifier channels (Kir) that have the ability to conduct currents in the inward direction and is involved in a salt bridge with an arginine residue (65). Asp-80 is conserved in voltage-gated Kv channels and involved in an H-bond with Trp-67 (4,66,67). The role played by negatively charged residues in the vicinity of the conductive pore in these channels remains to be understood.

CONCLUSIONS

QM/MM simulations were performed with the aim to assign the protonation state of the Glu-71 and Asp-80 residues in the KcsA channel x-ray structure. Calculations indicate that the protonation of Glu-71 is slightly favored over the protonation of Asp-80 but that the proton is exchanging between its two acceptors on the picosecond timescale, suggesting that a force field description of these interactions may lack the correct energetics. Analyzing the effect of the surrounding environment on the protonation state, an important aspect of the Asp/Glu motif has been identified, namely the dependence of the protonation state of the dyad on the position of the K^+ ions inside the selectivity filter. The interplay between the ionic binding sites and the location of the protons also implies that the energy profile for ion permeation in KcsA is influenced by the protonation state. The impact of these reciprocal effects on cations moving trough the selectivity filter is largest at the outer mouth ($\Delta E = \sim 8$ kcal/mol). It may suggest that the channel uses this mechanism to regulate the affinity for external channel blockers or to slow down inward currents. Inspection of the QM/MM MD trajectories revealed that also the salt bridge between Asp-80 and Arg-89 influences the proton transfer

probability. Thus, the mechanical response of the channel structure at distances as large as 10–20 Å from the ions in the selectivity filter could be coupled to ion translocation and to channel blocker binding. KcsA and KirBac channels may have evolved to make use of these reciprocal effects of the Glu/Asp protonation states on ion permeation energetics to assist their primordial function as regulators of ion homeostasis (63). The different tasks accomplished by eukaryotic channels, such as neural signaling, generation of the cardiac rhythm, signal transduction, and target cell lysis (68), coincide with the fact that the Asp/Glu motif is not generally conserved in these channels. Ultimately, understanding how negatively charged residues in the vicinity of conductive pores affect the ionic currents might lead to the design of new drugs that target channels with very high specificity (69).

REFERENCES

1. Tempel, B. L., Y. N. Jan, and L. Y. Jan. 1988. Cloning of a probable potassium channel gene from mouse brain. *Nature*. 332:837–839.

2. Hille, B. 2001. Ionic Channels of Excitable Membranes. Sinauer Associates, Sunderland, MA.

3. Doyle, D. A., J. M. Cabral, R. A. Pfuetzner, A. Kuo, J. M. Gulbis, S. L. Cohen, B. T. Chait, and R. MacKinnon. 1998. The Structure of the potassium channel: molecular basis of K^+ conduction and selectivity. *Science*. 280:69–77.

4. Jiang, Y. X., A. Lee, J. Y. Chen, V. Ruta, M. Cadene, B. T. Chait, and R. MacKinnon. 2003. X-ray structure of a voltage-dependent K^+ channel. *Nature*. 423:33–41.

5. Zhou, Y. F., J. H. Morais-Cabral, A. Kaufman, and R. MacKinnon. 2001. Chemistry of ion coordination and hydration revealed by a K^+ channel-Fab complex at 2.0 angstrom resolution. *Nature*. 414:43–48.

6. MacKinnon, R. 2003. Nobel Lecture. Potassium Channels and the Atomic Basis of Selective Ion Conduction. Bioscience Reports. The Nobel Foundation, Stockholm.

7. Zhou, Y. F., and R. MacKinnon. 2003. The occupancy of ions in the K^+ selectivity filter: charge balance and coupling of ion binding to a protein conformational change underlie high conduction rates. *J. Mol. Biol.* 333:965–975.

8. Aqvist, J., and V. Luzhkov. 2000. Ion permeation mechanism of the potassium channel. *Nature*. 404:881–884.

9. Ranatunga, K. M., I. H. Shrivastava, G. R. Smith, and M. S. P. Sansom. 2001. Side-chain ionization states in a potassium channel. *Biophys. J.* 80:1210–1219.

10. Chapman, M. L., M. L. Blanke, H. S. Krovetz, and A. M. J. VanDongen. 2006. Allosteric effects of external K^+ ions mediated by the aspartate of the GYGD signature sequence in the Kv2.1 K^+ channel. *Eur. J. Physiol.* 451:776–792.

11. Cordero-Morales, J. F., L. G. Cuello, and E. Perozo. 2006. Voltage-dependent gating at the KcsA selectivity filter. *Nat. Struct. Mol. Biol.* 13:319–322.

12. Cordero-Morales, J. F., L. G. Cuello, Y. Zhao, J. Vishwanath, D. M. Cortes, B. Roux, and E. Perozo. 2006. Molecular determinants of gating at the potassium-channel selectivity filter. *Nat. Struct. Mol. Biol.* 13:311–318.

13. Guidoni, L., V. Torre, and P. Carloni. 1999. Potassium and sodium binding to the outer mouth of the K^+ channel. *Biochemistry*. 38:8599–8604.

14. Heginbotham, L., E. Odessey, and C. Miller. 1997. Tetrameric stoichiometry of a prokaryotic K^+ channel. *Biochemistry*. 36:10335–10342.

15. Choi, H., and L. Heginbotham. 2004. Functional influence of the pore helix glutamate in the KcsA K^+ channel. *Biophys. J.* 86:2137–2144.

16. Cuello, L. G., J. G. Romero, D. M. Cortes, and E. Perozo. 1998. pH-dependent gating in the Streptomyces lividans K$^+$ channel. *Biochemistry*. 37:3229–3236.

17. Heginbotham, L., M. LeMasurier, L. Kolmakova-Partensky, and C. Miller. 1999. K$^+$ channel: functional asymmetries and sidedness of proton activation. *J. Gen. Physiol*. 114:551–560.

18. Domene, C., A. Grottesi, and M. S. P. Sansom. 2004. Filter flexibility and distortion in a bacterial inward rectifier K$^+$ channel: simulation studies of KirBac1.1. *Biophys. J*. 87:256–267.

19. VanDongen, A. M. J. 1992. Structure and function of ion channels: a hole in four? *Commun. Theor. Biol*. 2:429–451.

20. Chapman, M. L., H. M. A. VanDongen, and A. M. J. VanDongen. 1997. Activation-dependent subconductance levels in K channels suggest a subunit basis for ion permation and gating. *Biophys. J*. 72:708–719.

21. Berneche, S., and B. Roux. 2002. The ionization state and the conformation of Glu-71 in the KcsA K$^+$ channel. *Biophys. J*. 82:772–780.

22. Luzhkov, V. B., and J. Aqvist. 2005. Ions and blockers in potassium channels: insights from free energy simulations. *Biochim. Biophys. Acta*. 1747:109–120.

23. Crouzy, S., S. Berneche, and B. Roux. 2001. Extracellular blockade of K$^+$ channels by TEA: results from molecular dynamics simulations of the KcsA channel. *J. Gen. Physiol*. 118:207–217.

24. Berneche, S., and B. Roux. 2000. Molecular dynamics of the KcsA K$^+$ channel in a bilayer membrane. *Biophys. J*. 78:2900–2917.

25. Luzhkov, V. B., and J. Aqvist. 2001. K$^+$/Na$^+$ selectivity of the KcsA potassium channel from microscopic free energy perturbation calculations. *Biochim. Biophys. Acta*. 1548:194–202.

26. Compoint, M., P. Carloni, C. Ramseyer, and C. Girardet. 2004. Molecular dynamics study of the KcsA channel at 2.0 Angstrom resolution: stability and concerted motions within the pore. *Biochim. Biophys. Acta*. 1661:26–39.

27. Domene, C., P. J. Bond, and M. S. P. Sansom. 2003. Membrane protein simulations: ion channels and bacterial outer membrane proteins. *Protein Simulations*. 66:159–193.

28. Allen, T. W., S. Kuyucak, and S. H. Chung. 1999. Molecular dynamics study of the KcsA potassium channel. *Biophys. J*. 77:2502–2516.

29. Shrivastava, I. H., and M. S. P. Sansom. 2000. Simulations of ion permeation through a potassium channel: molecular dynamics of KcsA in a phospholipid bilayer. *Biophys. J*. 78:557–570.

30. Tieleman, D. P., P. C. Biggin, G. R. Smith, and M. S. P. Sansom. 2001. Simulation approaches to ion channel structure-function relationships. *Q. Rev. Biophys*. 34:473–561.

31. MacKerell, A. D., D. Bashford, M. Bellott, R. L. Dunbrack, J. D. Evanseck, M. J. Field, S. Fischer, J. Gao, H. Guo, S. Ha, D. Joseph-McCarthy, L. Kuchnir, et al. 1998. All-atom empirical potential for molecular modeling and dynamics studies of proteins. *J. Phys. Chem. B*. 102:3586–3616.

32. Varma, S., S. W. Chiu, and E. Jakobsson. 2006. The influence of amino acid protonation states on molecular dynamics simulations of the bacterial porin OmpF. *Bipohys. J*. 90:112–123.

33. Zhou, M., and R. MacKinnon. 2004. A mutant KcsA K$^+$ channel with altered conduction properties and selectivity filter ion distribution. *J. Mol. Biol*. 338:839–846.

34. Zhong, Q. F., Q. Jiang, P. B. Moore, D. M. Newns, and M. L. Klein. 1998. Molecular dynamics simulation of a synthetic ion channel. *Biophys. J*. 74:3–10.

35. Guidoni, L., V. Torre, and P. Carloni. 2000. Water and potassium dynamics inside the KcsA K$^+$ channel. *FEBS Lett*. 477:37–42.

36. Gross, A., L. Columbus, K. Hideg, C. Altenbach, and W. L. Hubbell. 1999. Structure of the KcsA potassium channel from Streptomyces lividans: a site-directed spin labeling study of the second transmembrane segment. *Biochemistry*. 38:10324–10335.

37. Darden T., D. York, and L. Pedersen. 1993. Particle mesh Ewald: a N·log(N) method for Ewald sums in large systems. *J. Chem. Phys*. 98:10089–10092.

38. Wang, J. M., R. M. Wolf, J. W. Caldwell, P. A. Kollman, and D. A. Case. 2004. Development and testing of a general amber force field. *J. Comput. Chem*. 25:1157–1174.

39. Car, R., and M. Parrinello. 1985. Unified approach for molecular-dynamics and density- functional theory. *Phys. Rev. Lett*. 55:2471–2474.

40. Hutter, J., A. Alavi, T. Deutch, M. Bernasconi, S. Goedecker, D. Marx, M. Tuckerman, and M. Parrinello. 1995–1999. CPMD. MPI für Festkörperforschung and IBM Zurich Research Laboratory. Available at: http://www.cpmd.org

41. Laio, A., J. VandeVondele, and U. Rothlisberger. 2002. A Hamiltonian electrostatic coupling scheme for hybrid Car-Parrinello molecular dynamics simulations. *J. Chem. Phys*. 116:6941–6947.

42. Kohn, W., and L. J. Sham. 1965. Self-consistent equations including exchange and correlation effects. *Phys. Rev*. 140:A1133–A1138.

43. Lee, C. T., W. T. Yang, and R. G. Parr. 1988. Development of the Colle-Salvetti correlation-energy formula into a functional of the electron-density. *Phys. Rev. B*. 37:785–789.

44. Becke, A. D. 1988. Density-functional exchange-energy approximation with correct asymptotic-behavior. *Phys. Rev. A*. 38:3098–3100.

45. Trouiller, N. J., L. Martins. 1991. Efficient pseudopotentials for plane-wave calculations. *Phys. Rev. B*. 43:8861–8869.

46. Frisch, M. J., G. W. Trucks, H. B. Schlegel, G. E. Scuseria, M. A. Robb, J. R. Cheeseman, J. Montgomery, J. A., T. Vreven, K. N. Kudin, J. C. Burant, J. M. Millam, S. S. Iyengar, et al. 2004. Gaussian 03, Revision C.02. Gaussian, Inc., Pittsburgh.

47. Fillaux, F., M. Limage, and F. Romain. 2002. Quantum proton transfer and interconversion in the benzoic acid crystal: vibrational spectra, mechanism and theory. *Chem. Phys*. 276:181–210.

48. Bucher, D., L. Guidoni, S. Raugei, M. Del Perraro, P. Carloni, and U. Rothlisberger. 2006. Polarization and charge transfer in a potassium channel. *J. Biophys. Chem*. 1241:292–301.

49. Guidoni, L., and P. Carloni. 2002. Potassium permeation through the KcsA channel: a density functional study. *Biochim. Biophys. Acta*. 1563:1–6.

50. Berneche, S., and B. I. Roux. 2005. A gate in the selectivity filter of potassium channels. *Structure*. 13:591–600.

51. VanDongen, A. 2004. K channel gating by an affinity-switching selectivity filter. *Proc. Natl. Acad. Sci. USA*. 9:3248–3252.

52. LeMasurier, M., L. Heginbotham, and C. Miller. 2001. KcsA: it's a potassium channel. *J. Gen. Physiol*. 118:303–313.

53. Hodgkin, A. L., and R. D. Keynes. 1955. The potassium permeability of a giant nerve fibre. *Journal of Physiology-London*. 128:61–88.

54. Immkea, D., and J. S. Korna. 2000. Evidence from K$^+$ dependent modulation of tetraethylammonium efficacy in Kv2.1 potassium channels. *J. Gen. Physiol*. 115:509–518.

55. Yang, Y., and C. Kuo. 2005. An inactivation stabilizer of the Na$^+$ channel acts as an opportunistic pore blocker modulated by external Na$^+$. *J. Gen. Physiol*. 125:465–481.

56. Heginbotham, L., and E. Kutluay. 2004. Revisiting voltage-dependent relief of block in ion channels: a mechanism independent of punchthrough. *Biophys. J*. 86:3663–3670.

57. Schrempf, H., O. Schmidt, R. Kummerlen, S. Hinnah, D. Muller, M. Betzler, T. Steinkamp, and R. Wagner. 1995. A prokaryotic potassium ion channel with two predicted transmembrane segments from *Streptomyces lividans*. *EMBO J*. 14:5170–5178.

58. Heginbotham, L., L. Kolmakova-Partensky, and C. Miller. 1998. Functional reconstitution of a prokaryotic K1 channel. *J. Gen. Physiol*. 111:741–749.

59. Jiang, C., Z. Qu, and H. Xu. 2002. Gating of inward rectifier K$^+$ channels by proton-mediated interactions of intracellular protein domains. *Trends Cardiovasc. Med*. 12:5–13.

60. Jiang, Y., A. Lee, J. Chen, M. Cadene, B. T. Chait, and R. MacKinnon. Crystal structure and mechanism of a calcium-gated potassium channel. 2002. *Nature*. 417:515–522.

61. Haug, T., D. Sigg, S. Ciani, L. Toro, E. Stefani, and R. Olcese. 2004. Regulation of K^+ flow by a ring of negative charges in the outer pore of BKca channels. Part I. Aspartate 292 modulates K^+ conduction by external surface charge effect. *J. Gen. Physiol.* 124:173–184.

62. Wang, Y., L. Xu, D. A. Pasek, D. Gillespie, and G. Meissner. 2005. Probing the role of negatively charged amino acid residues in ion permeation of skeletal muscle ryanodine receptor. *Bipohys. J.* 89:256–265.

63. Miller, C. 2000. An overview of the potassium channel family. *Genome Biol.* 1:4.

64. Shealy, R. T., A. D. Murphy, R. Ramarathnam, E. Jakobsson, and S. Subramaniam. 2003. Sequence-function analysis of the K^+-selective family of ion channels using a comprehensive alignment and the KcsA channel structure. *Biophys. J.* 84:2929–2942.

65. Yang, J., M. Yu, Y. N. Jan, and L. Y. Jan. 1997. Stabilization of ion selectivity filter by pore loop ion pairs in an inwardly rectifying potassium channel. *Proc. Natl. Acad. Sci. USA.* 94:1568–1572.

66. Sigworth. 1997. How does the W434F mutation block current in Shaker potassium channels? *J. Gen. Physiol.* 109:779–789.

67. Long, S. B., E. B. Campbell, and R. MacKinnon. 2005. Crystal structure of a mammalian voltage-dependent Shaker family K^+ channel. *Science.* 309:897–903.

68. Attali, B., G. Romey, E. Honore, A. Schmid-Alliana, M. Mattei, F. Lesage, P. Ricard, J. Barhanin, and M. Lazdunski. 1992. Cloning, functional expression, and regulation of two K^+ channels in human T lymphocytes. *J. Biol. Chem.* 12:8650–8657.

69. Sanguinetti, M. C., and P. B. Bennett. 2003. Antiarrhythmic drug target choices and screening. *Circ. Res.* 93:491–499.